



## Original Research Article

View Article Online | View Journal

## Pd Catalyst Supported Thermo-Responsive Modified Poly(*N*-isopropylacrylamide) Grafted Fe<sub>3</sub>O<sub>4</sub>@CQD@Si in Heck Coupling Reaction

Soheila Ghasemi\* , Fatemeh Badri, Hadieh Rahbar Kafshboran

Department of Chemistry, College of Sciences, Shiraz University, Shiraz 7194684795, Iran

## ARTICLE INFORMATION

Submitted: 22 June 2023  
 Revised: 20 August 2023  
 Accepted: 21 August 2023  
 Available online: 28 August 2023

Manuscript ID: [AJGC-2307-1401](#)

Checked for Plagiarism: Yes

Language Editor:

[Dr. Fatimah Ramezani](#)

Editor who approved publication:

[Dr. Ali Ramazani](#)

DOI: 10.48309/ajgc.2024.408188.1401

## KEYWORDS

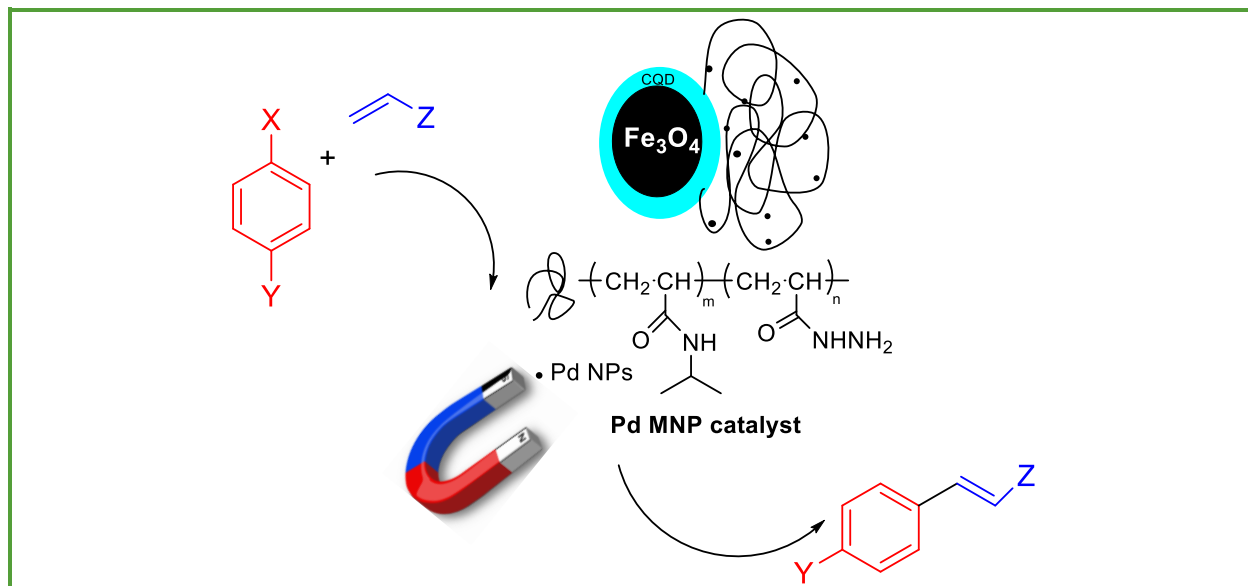
Thermo-responsive polymers  
 PNIPAM  
 Pd catalyst  
 Mizoroki-Heck coupling

## ABSTRACT

A new smart Pd catalyst was created based on functionalized thermo-responsive poly (*N*-isopropylacrylamide) (PNIPAM) grafted Fe<sub>3</sub>O<sub>4</sub>@CQD@Si. For catalyst fabrication, initially, Fe<sub>3</sub>O<sub>4</sub> magnetic nanoparticle was prepared by co-precipitation method, and then it was coated with CQD as sustainable and environmentally friendly support. Chemical modification of Fe<sub>3</sub>O<sub>4</sub>@CQD support with polymerizable groups was performed through vinyltriethylsilan (VTES) reaction. Thereafter, PNIPAM was grafted to the modified Fe<sub>3</sub>O<sub>4</sub> via the conventional free radical polymerization technique. The PNIPAM-grafted Fe<sub>3</sub>O<sub>4</sub>@CQD@Si was further treated using hydrazine to create the modified amino support, which was then complexed with Pd(OAc)<sub>2</sub> to yield the magnetic heterogeneous catalytic system. All materials are characterized using various methods, *i.e.*, FT-IR, SEM, DLS, CHN, XRD, zeta potential, VSM, and TGA analysis techniques. Fe<sub>3</sub>O<sub>4</sub>@CQD@Si@PNIPAM-NH<sub>2</sub>/Pd catalyst was used to produce a range of substituted alkenes in the Mizoroki-Heck cross-coupling reaction with a high turnover number (TON) and good to outstanding yields. Above the LCST temperature of the PNIPAM, the hydrophobic part of the polymer starts to shrink, and this smart catalyst advances the relevant reactions in milder conditions. Easy purification of the substituted alkenes due to the convenient isolation of the magnetic catalyst with an external magnet is the main characteristic of this process.

© 2024 by SPC (Sami Publishing Company), Asian Journal of Green Chemistry, Reproduction is permitted for noncommercial purposes.

## Graphical Abstract



## Introduction

One of the noteworthy and broadly applied transformations for the creation of bonds between carbon atoms is the Heck reaction, allowing various alkenes to get vinylylated, arylated, or alkylated mildly in a single step by reacting them with benzyl, vinyl, aryl, acetates, triflates, or allyl halides applying Pd catalyst and an appropriate base [1]. Palladium is one of the most effective metals for catalyzing the C-C bonds coupling reactions and has recently gained a great deal of interest [2]. Pd NPs are a viable option in searching for mild reaction conditions and more environmentally friendly procedures because of their great surface-to-volume ratio and incredibly reactive surface atoms compared to the bulk catalyst atoms. The Pd<sup>II</sup>/Pd<sup>0</sup> complexes conventionally catalyze coupling reactions in the presence of phosphines or other ligands. Consequently, using Pd NPs enables "ligand-free" synthesis, which reduces costs, simplifies the procedure and facilitates the separation of the resulting product [3-5].

Several homogeneous catalytic systems for the Heck reaction have been reported, but all

suffer from poor catalyst separation and recycling, and attempts have been made to successfully resolve the difficulties using heterogeneous catalysts with high activity and minimum leaching [6-8]. Palladium species have been immobilized through a variety of solid supports [9], including magnetic nanoparticles [9], silica gel [11], MOs (metal oxides) [12], MOFs (metal-organic frameworks) [13], CNTs (carbon nanotubes) [14], zeolite [15], alumina [16], graphene [17], and polymers [18]. The use of polymer-bonded NPs takes advantage of the linear polymers, such as excellent thermal and mechanical durability, as well as excellent dispersion provided by nano particles [19, 20]. Similarly, covering Fe<sub>3</sub>O<sub>4</sub> NPs with silica shells and producing magnetic core-shell nanocomposites can prevent aggregation of Fe<sub>3</sub>O<sub>4</sub> NPs and enhance their dispersion, as well as affect surface property and coupling with functional groups arising from polymer components [21-24].

Many studies have reported the high performance of palladium-iron oxide (Pd-Fe<sub>3</sub>O<sub>4</sub>) systems in the Heck coupling reaction due to its excellent catalytic properties of Pd and

magnetically recoverable feature of  $\text{Fe}_3\text{O}_4$ .  $\text{Fe}_3\text{O}_4/\text{SiO}_2$ -Pd magnetic nanocatalyst with multibranched polyglycerol was created by Zhou *et al.* and demonstrated high catalytic activity in Heck reaction [25]. Bian and *et al.* synthesized a hybrid magnetic inorganic/responsive organic polymer nanocomposite *via* free radical polymerization of sodium acrylate (SAA), 4-vinyl pyridine (4-VP), and undecylenic acid (UDA) onto  $\text{Fe}_3\text{O}_4$ . The magnetic nanocomposite  $\text{Fe}_3\text{O}_4@P(\text{UDA-co-4-VP-co-SAA})$  ( $\text{Fe}_3\text{O}_4@PUVS$ ) decorated by Pd to fabricate the  $\text{Fe}_3\text{O}_4@PUVS$ -Pd nano catalyst, and revealed outstanding catalytic activity in the Suzuki and Heck C-C cross-coupling reactions in aqueous media [26]. Ramazani *et al.* prepared a robust magnetic palladium catalyst based on artificial metalloenzyme. The catalyst is synthesized through anchoring  $\text{Pd}(2,2'\text{-dipyridylamine})\text{Cl}_2$  supported monomethyl ether poly(ethylene glycol) (mPEG) onto amino modified silica-coated  $\text{Fe}_3\text{O}_4$  NPs and demonstrated impressive catalytic activity in Suzuki C-C coupling reaction [27].

As part of our ongoing investigation on Pd catalysts integrated into polymer-grafted silica [28-31], the present work is focused on synthesizing and characterizing a magnetic well defined amino modified thermo-responsive poly (*N*-isopropylacrylamide) (PNIPAM).

Afterwards,  $\text{Pd}(\text{OAc})_2$  complexation of this ligand after adding  $\text{NaBH}_4$  as a reducing agent was performed to achieve the supported catalyst for manufacturing diversely substituted alkenes in Mizoroki-Heck cross-coupling transformation with good to excellent yield and high turnover number (TON).

## Experimental

### Materials

Azobisisobutyronitrile (AIBN, Merck, 98%) was refined using methanol through

recrystallization. *N*-Isopropylacrylamide (NIPAM) (Acros, 99%) was recrystallized utilizing *n*-hexane. Citric acid (Sigma-Aldrich 99.5%), vinyltrimethoxysilane (VTES, Sigma-Aldrich, 98%), hydrazine hydrate (Merck, 80% solution in water), and ethylenediamine (Merck, 99%) were used without further purification. 1,4-Dioxane (Sigma-Aldrich,  $\geq 99\%$ ) was dried initially utilizing a molecular sieve as preliminary drying agent. The ultimate drying has been performed nearly completely through the distillation of a refluxed solution in the presence of 1% w/v sodium wire prepared with sodium press and 0.2% w/v benzophenone till the benzophenone ketyl radical anion's blue color emerges under an inert environment. Palladium (II) acetate ( $\text{Pd}(\text{OAc})_2$ , 98%, 47% Pd) was purchased from Sigma Aldrich.

### Characterization techniques

FT-IR 8300 spectrophotometer-Shimadzu was used to record FT-IR data. To prepare samples, KBr was used for compacting them into a pellet. Bruker Avance DPX instrument (250 MHz in  $\text{CDCl}_3$ ) was employed to obtain NMR spectra of the coupling products. To achieve the XRD patterns of MNP and their modified forms, Bruker AXS D8-Advance X-ray diffractometer ( $\lambda = 1.541874 \text{ \AA}$  for Cu  $K\alpha$  radiation and  $2\theta = 10\text{-}90^\circ$ ) was used. An Elemental (CHN) analyzer, LCHN-A10, was applied to measure the amount of carbon, hydrogen, and nitrogen in each sample. The photoluminescence spectrum was derived from a FluoroMax-4 fluorescence spectrometer at an excitation wavelength of 350 nm. Thin-layer chromatography was carried out using silica-gel plates (polygram SIL-UV 254). Scanning electron micrographs were obtained with VEGA3 TESCAN SEM at 20 kV. Gold was sputter-coated onto the specimens to increase the conductivity by KYKY SBC12 sputter coater by applying physical vapor deposition (PVD) technique before SEM analysis. Polymer

hydrodynamic sizes were determined using SZ-100 dynamic light scattering (DLS) from aqueous samples with concentration of 1 mg/mL in 2 mL microtubes. Zeta seizer (ZETA-check Particle Charge Reader, Horiba Jobin Jyovin) was applied to estimate the surface charge of the polymer. The amount of grafted PNIPAM onto  $\text{Fe}_3\text{O}_4$  MNPs was determined by Perkin Elmer Pyris Diamond thermogravimetric analyzer (TGA). Before TGA analysis, the samples were dried under a vacuum overnight and next scanned at a heating rate of  $5\text{ }^\circ\text{C min}^{-1}$  under  $\text{N}_2$  inert gas flow between  $25\text{ }^\circ\text{C}$  to  $700\text{ }^\circ\text{C}$ . Platinum pans were used to analyze samples weighing between 1.5 to 3.5 mg. The saturation magnetizations of bare and surface-functionalized  $\text{Fe}_3\text{O}_4$  MNPs were explored by a vibrating sample magnetometer (magnetic daghigh kavir VSM) and samples weighing around 200 mg were used. The Pd amount determination was performed by an inductively coupled plasma implement (Varian, Vista-Pro ICP-OES).

#### *Preparation of super paramagnetic $\text{Fe}_3\text{O}_4$ (I)*

In distilled water (40 mL), a combination of  $\text{FeCl}_2\cdot 4\text{H}_2\text{O}$  (4.73 mmol, 0.93 g) and  $\text{FeCl}_3\cdot 6\text{H}_2\text{O}$  (9.46 mmol, 2.5 g) salts were dissolved. After 15 minutes of ultrasonication, the mixture was transferred to a 250 mL three-necks, round bottom flask equipped with a separatory funnel containing NaOH (40 mL, 1 M) under an Ar environment. During the gradual co-precipitation process, NaOH was added dropwise into the mixture throughout 90 minutes to generate  $\text{Fe}_3\text{O}_4$  nuclei. To grow  $\text{Fe}_3\text{O}_4$  particles with a spherical form and regulate particle size, the pH of the reaction solution was maintained between 10 to 12. The as-prepared, black product was separated using a small magnet bar, washed multiple times in distilled  $\text{H}_2\text{O}$  and EtOH, and next vacuum-dried at  $50\text{ }^\circ\text{C}$  for 9 hours.

#### *Preparation of CQD suspension*

As reported previously, amino-rich fluorescent CQD was created by pyrolyzing citric acid and ethylenediamine with the aid of a microwave. Citric acid (1 g, 5.20 mmol) was dissolved in 20 mL water and next, ethylenediamine (0.4679 g, 7.785 mmol) was introduced to produce a transparent and clear solution while stirring vigorously. The solution was then located for 4 minutes in a 700 W microwave oven. The resultant black-brown CQD aqueous solution was cooled to room temperature.

#### *Preparation of CQD coated $\text{Fe}_3\text{O}_4$ MNP ( $\text{Fe}_3\text{O}_4\text{@CQD}$ ) (II)*

The as-prepared  $\text{Fe}_3\text{O}_4$  nanoparticle (0.25 g) was sonicated in water (3 mL) for 10 minutes and next added to the flask with 3.5 mL of the CQD suspension. The suspension was continuously stirred at  $60\text{ }^\circ\text{C}$  for 1 day. Afterwards, the synthesized  $\text{Fe}_3\text{O}_4\text{@CQD}$  (II) was separated magnetically, and the product was washed multiple times in distilled  $\text{H}_2\text{O}$  and EtOH before being vacuum-dried.

#### *Preparation of VTES coated $\text{Fe}_3\text{O}_4\text{@CQD}$ ( $\text{Fe}_3\text{O}_4\text{@CQD@Si}$ ) (III)*

Silica-modified magnetite nanoparticle with polymerizable double bonds was produced by treating VTES with the hydroxyl groups on the surface of  $\text{Fe}_3\text{O}_4\text{@CQD}$ . A homogenous suspension was obtained by sonicating 1.0 g of  $\text{Fe}_3\text{O}_4\text{@CQD}$  NPs in 60 mL of EtOH for approximately one hour and then 12 mL of  $\text{NH}_3\cdot\text{H}_2\text{O}$  was added. VTES (6 mL) was introduced to the suspension while constantly stirring for 1 day at  $50\text{ }^\circ\text{C}$ . The product ( $\text{Fe}_3\text{O}_4\text{@CQD@Si}$ ) was then separated using a magnet bar and extensively washed with distilled  $\text{H}_2\text{O}$  and EtOH until neutralized and

finally vacuum-dried at ambient temperature overnight.

*Preparation of thermo-responsive PNIPAM brushes grafted onto modified Fe<sub>3</sub>O<sub>4</sub> MNP (Fe<sub>3</sub>O<sub>4</sub>@CQD@Si@PNIPAM) (IV)*

In a polymerization tube containing stirrer, azobisisobutyronitrile (AIBN) (0.017 mmol, 2.90 mg) as initiator, *N*-isopropylacrylamide (8.83 mmol, 1.00 g) as monomer (molar ratio of monomer: AIBN = 150: 0.3) and Fe<sub>3</sub>O<sub>4</sub>@CQD@Si (386 mg) were introduced, and then 1.5 mL dry 1,4-dioxane was added. Thereafter, the tube was immersed in liquid nitrogen until the contents were frozen, and then vacuumed for a few minutes to degas. After sealing the polymerization tube, it was heated in oil bath at 85 °C with vigorous stirring for 1 day. Following magnetic separation using a permanent magnet, the resulting product (Fe<sub>3</sub>O<sub>4</sub>@CQD@Si@PNIPAM) was completely washed with 1,4-dioxane and vacuum-dried for 24 h at 50 °C.

*Preparation of Fe<sub>3</sub>O<sub>4</sub>@CQD@Si@PNIPAM-NH<sub>2</sub> (V)*

Compound (IV) (1.38 g) was added gradually to an excess amount of hydrazine monohydrate. (7 ml) in 5 mL 1, 4-dioxane. The suspension was heated for 9 h at 90 °C while thoroughly stirring. A permanent magnet was used for the magnetic separation to obtain the desired amino-modified compound (Fe<sub>3</sub>O<sub>4</sub>@CQD@Si@PNIPAM-NH<sub>2</sub>). The product was washed thoroughly with 1,4-dioxane and then vacuum dried at 60 °C.

*Preparation of Pd catalyst (Fe<sub>3</sub>O<sub>4</sub>@CQD@Si@PNIPAM-NH<sub>2</sub>/Pd) (VI)*

In a reaction flask, the compound (V) (0.22 g) was dispersed in EtOH (4 mL) and then Pd(OAc)<sub>2</sub> (0.224 g, 1 mmol) was introduced. The suspension was stirred at ambient temperature

for 12 h. The corresponding mixture was next gathered by a permanent magnet and next dried under vacuum overnight. Pd<sup>0</sup> NPs supported on Fe<sub>3</sub>O<sub>4</sub>@CQD@Si@PNIPAM-NH<sub>2</sub> were yielded by adding NaBH<sub>4</sub> (10 mg, 0.264 mmol) as a reductant. The magnetic heterogeneous catalytic system was obtained through the complexation of the amino-modified support with Pd. Magnetic separation with a permanent magnet yielded the desired product, which was then vacuum-dried. To measure the Pd loading, the compound (VI) was digested successively in distilled water, HCl and HNO<sub>3</sub> (2:1:1) and subjected to ICP. Pd loading was found to be 1.1 mmol of Pd per gram of heterogenous catalyst.

*General approach for the Mizoraki-Heck coupling using Pd catalyst (VI)*

In a round-bottom flask, a haloarene (1 mmol), K<sub>2</sub>CO<sub>3</sub> (2 mmol), and Pd catalyst (VI) (5 mg, 0.55 mol%) were mixed with DMF (2 mL), and then styrene or *n*-butylacrylate (1.5 mmol) was introduced to the previous suspension. The suspension was heated at 95 °C with constant stirring for a required time. TLC was used to monitor the reaction. Once the coupling reaction was completed, the suspension cooled to ambient temperature. The catalyst (VI) was simply separated magnetically and the remaining solution was extracted with EtOAc several times. The organic phases were combined, and then evaporated under reduced pressure after drying over anhydrous MgSO<sub>4</sub>. Purification of the coupling products was then performed using plate chromatography on silica gel with petroleum ether (90): ethyl acetate (10) as the eluent and giving the desired products in 85 to 95% isolated yield. To characterize the coupling products, their spectroscopic data (FT-IR and <sup>1</sup>H-NMR) were compared with authentic samples.

## Results and Discussion

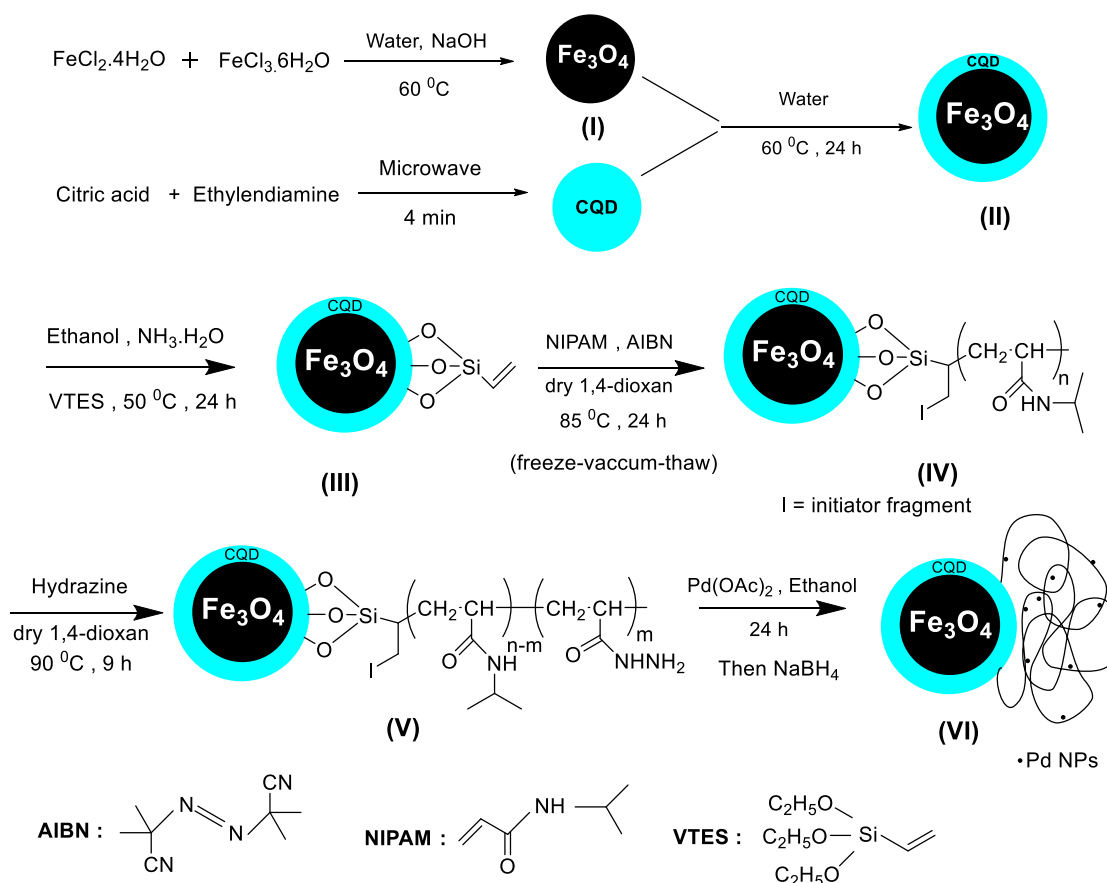
Preparation and characterization of  $Fe_3O_4@CQD@Si@PNIPAM-NH_2/Pd$  catalyst

A thermo-responsive palladium catalyst supported on PNIPAM grafted  $Fe_3O_4@CQD@Si$  was prepared as depicted schematically in Scheme 1.  $Fe_3O_4$  superparamagnetic nanoparticle (I) was created using salts of  $Fe^{2+}$  and  $Fe^{3+}$  by the co-precipitation procedure. Prepared  $Fe_3O_4$  nanoparticles were coated with synthesized CQD as the fluorescent agent. CQDs are safe and environmentally friendly for use in medicine and biology, because they release

intense fluorescence like QDs and are nontoxic and cheap.

Low toxicity, huge specific surface area, adjustable bandgap, excellent solubility, intense and consistent photoluminescence, and good biocompatibility give CQDs higher economic value than the other QDs, and as a result, they can be utilized as environmentally friendly and sustainable support for coating MNPs [32].

Next, the CQD-modified  $Fe_3O_4$  NP reacted with vinyltriethylsilane (VTES) to form compound (III) ( $Fe_3O_4@CQD@Si$ ) to modify the surface of MNPs by adding polymerizable double bond groups.



**Scheme 1.** Schematic illustration for the synthesis of  $Fe_3O_4@CQD@Si@PNIPAM-NH_2/Pd$  catalyst

Thereafter, PNIPAM bonded  $Fe_3O_4$  magnetic nanoparticles ( $Fe_3O_4@CQD@Si@PNIPAM$ ) (IV) were synthesized using AIBN as initiator and

NIPAM as monomer in dry and degassed 1,4-dioxane, through conventional free radical polymerization technique. Finally, the PNIPAM

grafted  $\text{Fe}_3\text{O}_4@\text{CQD}@\text{Si}$  was modified with hydrazine to transform it to amino-functionalized compound. Eventually, this compound (V) was complexed with  $\text{Pd}(\text{OAc})_2$  and after the  $\text{NaBH}_4$  addition as a reducing agent, produce compound (VI) ( $\text{Fe}_3\text{O}_4@\text{CQD}@\text{Si}@\text{PNIPAM-NH}_2/\text{Pd NP}$ ) in the form of a magnetic heterogeneous catalyst. The optical property of the CQD was evaluated by fluorescence spectroscopy, which revealed two prominent peaks, one at approximately 226 nm owing to the  $\pi$  to  $\pi^*$  transition of carbon-carbon and the other at approximately 350 nm due to the  $n$  to  $\pi^*$  transitions of C=N and C-O. CQDs were excited most efficiently and showed strong blue fluorescence at 360 nm (Figure 1).

FT IR spectra of all synthesized compounds ( $\text{Fe}_3\text{O}_4$  (I),  $\text{Fe}_3\text{O}_4@\text{CQD}$  (II),  $\text{Fe}_3\text{O}_4@\text{CQD}@\text{Si}$  (III),  $\text{Fe}_3\text{O}_4@\text{CQD}@\text{Si}@\text{PNIPAM}$  (IV), and  $\text{Fe}_3\text{O}_4@\text{CQD}@\text{Si}@\text{PNIPAM-NH}_2/\text{Pd}$  (VI)) are gathered and confirmed their structures (Figure 2). FT IR spectrum of  $\text{Fe}_3\text{O}_4$  NPs revealed the

absorption peak at  $588\text{ cm}^{-1}$  assign to the stretching vibration of Fe-O bonds and, the broad peak at about  $3441\text{ cm}^{-1}$  is related to O-H stretching of bare  $\text{Fe}_3\text{O}_4$  NPs (I) (Figure 2a). The FT-IR spectrum of the  $\text{Fe}_3\text{O}_4@\text{CQD}$  (II) showed the typical absorption of the  $-\text{NH}_2$  at  $1407\text{ cm}^{-1}$  and  $1180\text{ cm}^{-1}$ , and  $-\text{OH}$  hydroxyl group at  $3437\text{ cm}^{-1}$  (Figure 2b). In the FT-IR spectrum of  $\text{Fe}_3\text{O}_4@\text{CQD}@\text{Si}$  (III), frequencies of Si-O-Si and Si-O stretching vibrations emerged at  $1134$  and  $1051\text{ cm}^{-1}$ , respectively, which validate the reaction between hydroxyl groups on the  $\text{Fe}_3\text{O}_4$  surface with VTES (Figure 2c). The FT IR spectrum for  $\text{Fe}_3\text{O}_4@\text{CQD}@\text{Si}@\text{PNIPAM}$  (IV) shows expected bands at  $3435\text{ cm}^{-1}$  (N-H),  $1634\text{ cm}^{-1}$  (C=O),  $2975$  and  $1386\text{ cm}^{-1}$  (C-H bonding) and matching well to the expected structure of the polymer (Figure 2d). The FT-IR spectrum of compound (VI) exhibited the typical absorption of C=O group at  $1644\text{ cm}^{-1}$ ,  $-\text{OH}$  hydroxyl group at  $3435\text{ cm}^{-1}$ , and aliphatic group C-H at  $2964\text{ cm}^{-1}$  and  $2923\text{ cm}^{-1}$  (Figure 2e).

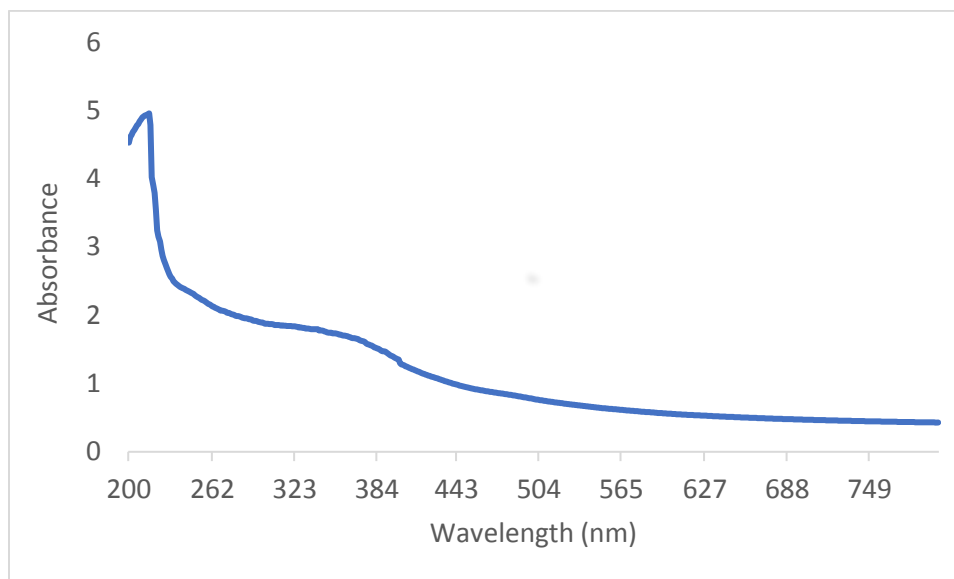


**Figure 1.** Fluorescence spectrum of  $\text{Fe}_3\text{O}_4@\text{CQD}$

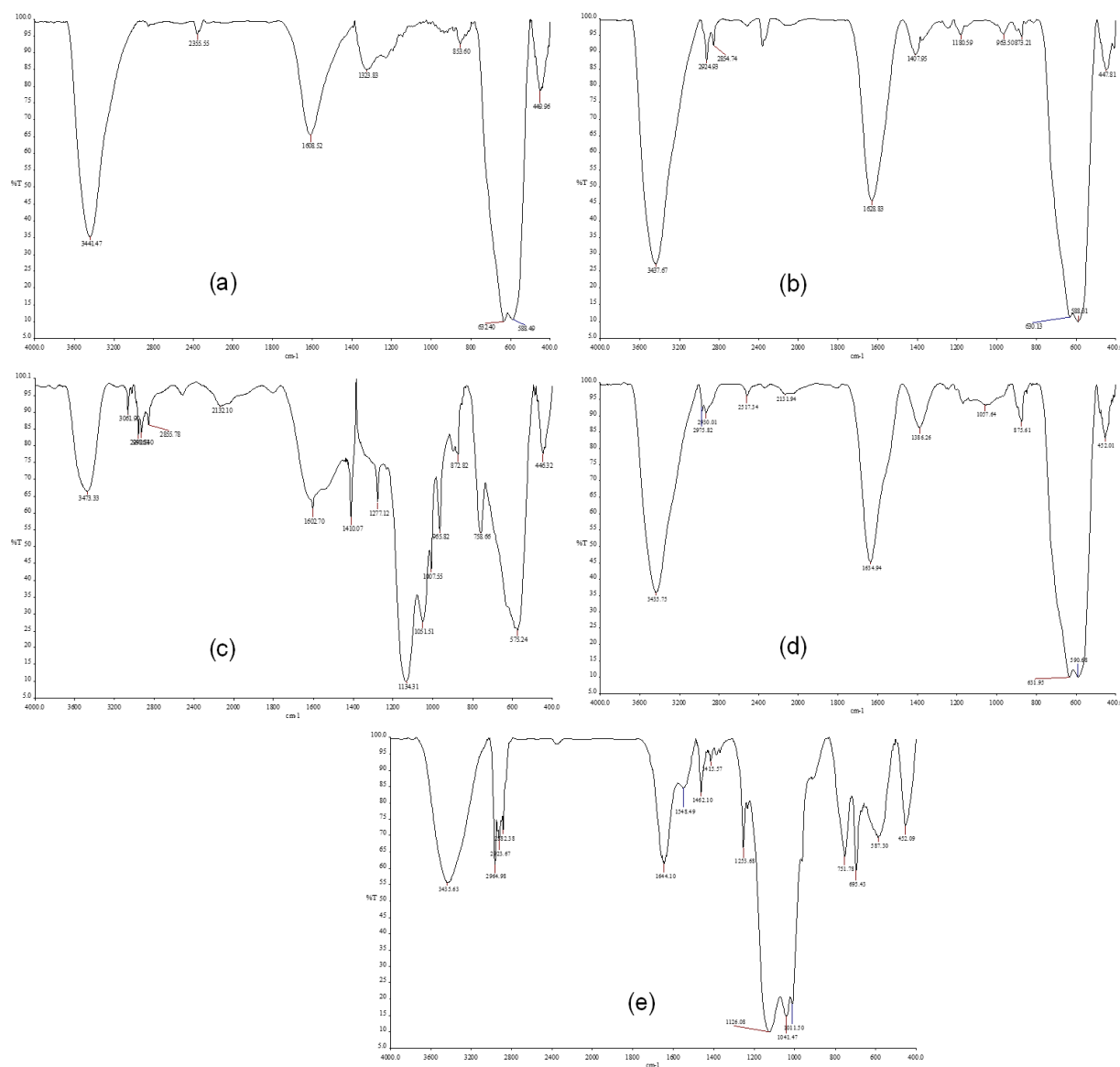


**Figure 2.** (a) FT-IR spectra of (a)  $\text{Fe}_3\text{O}_4$  MNPs (I), (b)  $\text{Fe}_3\text{O}_4$ @CQD (II), (c)  $\text{Fe}_3\text{O}_4$ @CQD@Si (III), (d)  $\text{Fe}_3\text{O}_4$ @CQD@Si@PNIPAM (IV), and (e)  $\text{Fe}_3\text{O}_4$ @CQD@Si@PNIPAM@hydrazine/Pd (VI)

By comparison of magnetic properties of compounds (I) and (IV) by vibration sample magnetometry (VSM), the saturation of the nanoparticles decreased from 150 emu/g for untreated  $\text{Fe}_3\text{O}_4$  (I) to 25 emu/g for the  $\text{Fe}_3\text{O}_4$ @CQD@Si@PNIPAM nanoparticle (IV) (Figure 3). This drop in saturation might result from the surface coating and functionalization of  $\text{Fe}_3\text{O}_4$  nanoparticles with polymer chains.

By checking the thermogravimetric analysis (TGA) of compounds (I) and (IV), we can see that the uncoated nanoparticles were thermally stable. Approximately, 85% mass loss of compound (IV) is occurred at two main pyrolysis stages during thermal degradation of organic segments. This compound exhibited good thermal stability under 500 °C, and all organic materials were destroyed completely at about 750 °C (Figure 4).



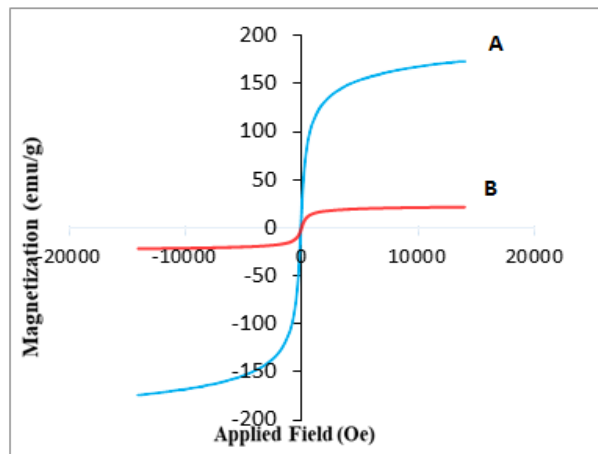


**Figure 3.** VSM curves for the prepared (A) bare  $\text{Fe}_3\text{O}_4$  (I) and (B)  $\text{Fe}_3\text{O}_4@\text{CQD}@\text{Si}@\text{PNIPAM}$  (IV)

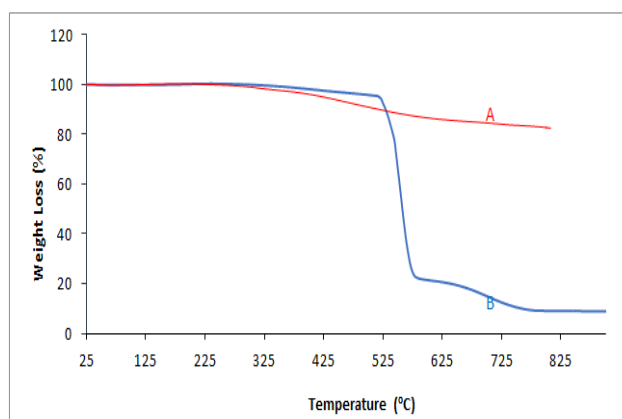


**Figure 4.** TGA curves for the prepared bare (A)  $\text{Fe}_3\text{O}_4$  (I) and (B)  $\text{Fe}_3\text{O}_4@\text{CQD}@\text{Si}@\text{PNIPAM}$  (IV)

The LCST of thermoresponsive compounds (IV, V, and VI) was measured by heating the samples and record the temperature at which they begin to shrink. Compounds IV, V, and VI have LCST of approximately 33 °C, 36 °C, and 40 °C, respectively. The increase in LCST from compound (IV) to compound (V) is due to the increase in hydrophilicity of layers. One of the reasons for choosing PNIPAM in the catalyst' structure is due to the fact that hydrophobic portion of PNIPAM begins to shrink after the LCST and the corresponding catalytic reaction in this portion is carried out under mild conditions.

The results of CHNS analysis of compounds at various steps of catalyst synthesis were

measured, and the increase in the proportion of nitrogen, hydrogen, and carbon content shows the growth of polymer chains and the formation of organic components onto the MNPs.

SEM images were utilized to assessed the morphology and size of the uncoated and coated MNPs' surfaces. The majority of the uncoated nanoparticles are quasi-spherical and have mean sizes of about 0.05  $\mu\text{m}$ , as demonstrated in [Figure 5](#). Aggregation was decreased, and nanoparticle dispersion was enhanced after polymer coating. The absence of particle aggregation is likely due to the VTES and PNIPAM coatings, which reduce magnetic interactions between particles ([Figure 5](#)).

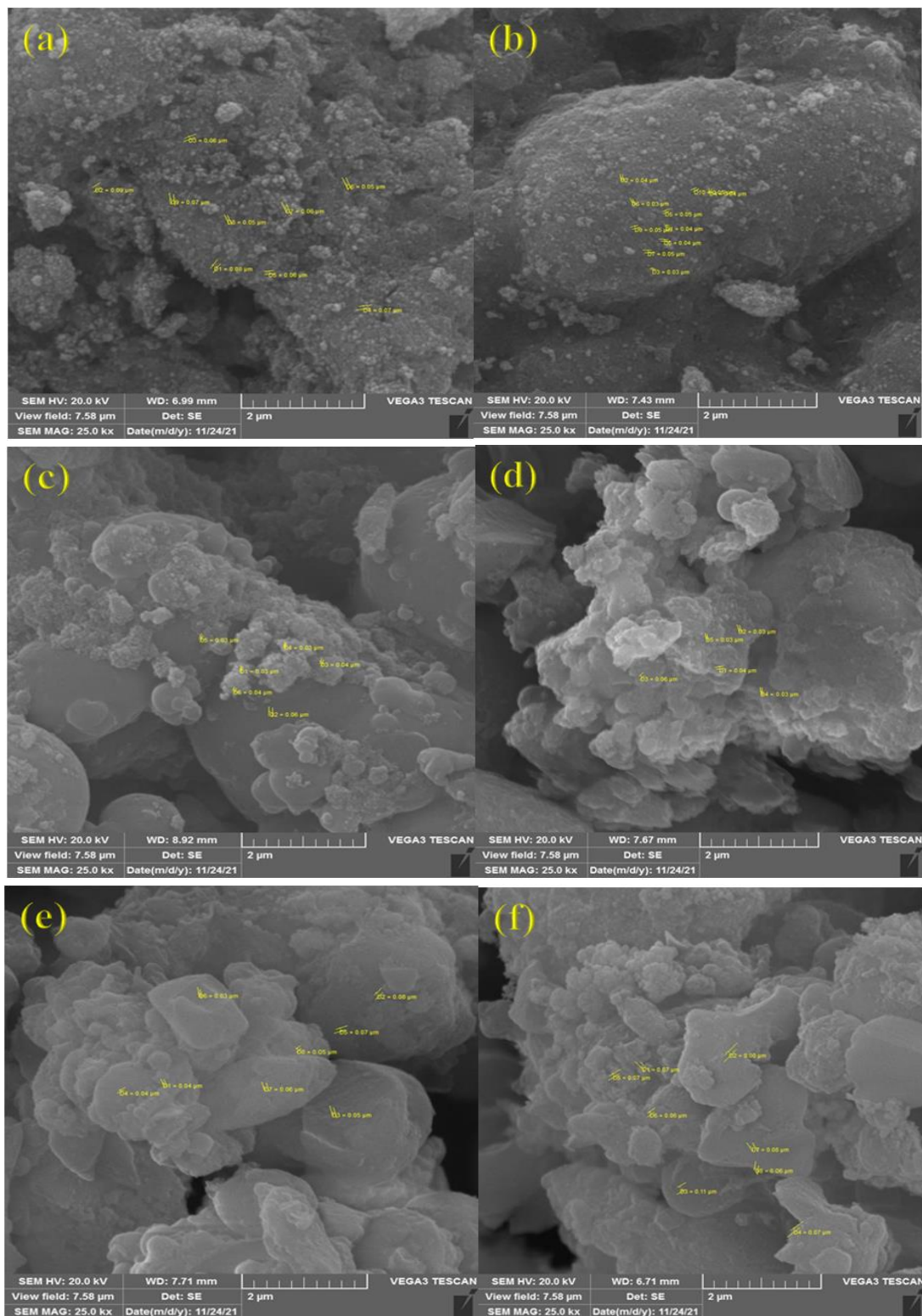


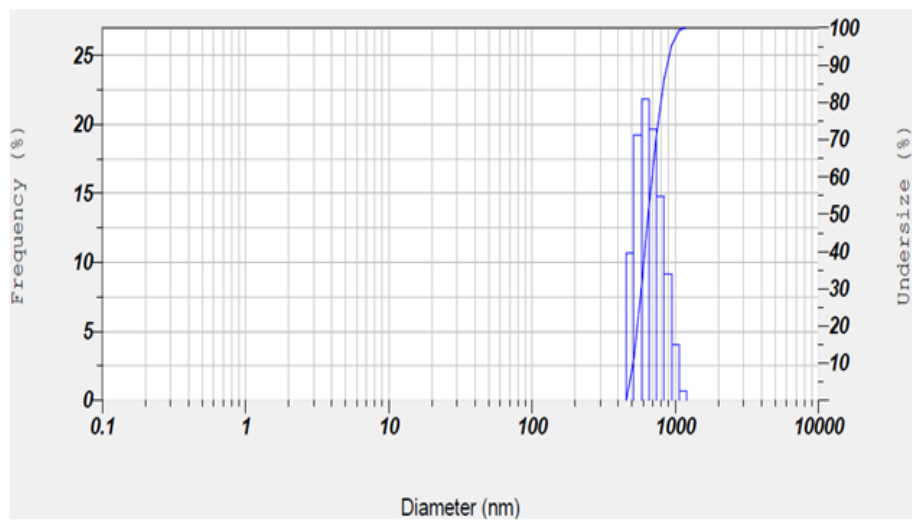
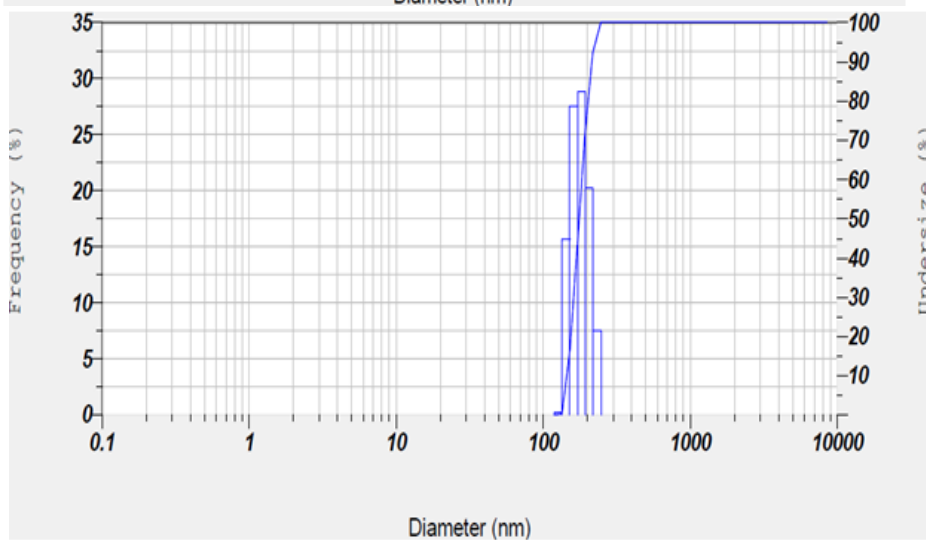
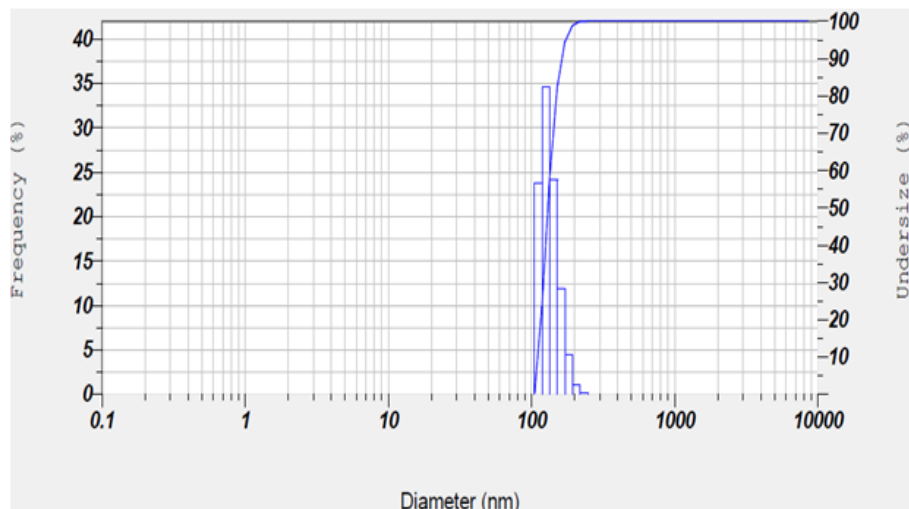
**Figure 5.** SEM images of (a) Fe<sub>3</sub>O<sub>4</sub> MNPs (I), (b) Fe<sub>3</sub>O<sub>4</sub>@CQD (II), (c) Fe<sub>3</sub>O<sub>4</sub>@CQD@Si (III), (d) Fe<sub>3</sub>O<sub>4</sub>@CQD@Si@PNIPAM (IV), (e) Fe<sub>3</sub>O<sub>4</sub>@CQD@Si@PNIPAM-NH<sub>2</sub> (VI), and (f) Fe<sub>3</sub>O<sub>4</sub>@CQD@Si@PNIPAM-NH<sub>2</sub>/Pd (V)

DLS test was applied to measure the hydrodynamic diameter of bare  $\text{Fe}_3\text{O}_4$  and their modified forms (Figure 6). The size distribution graphs for the naked  $\text{Fe}_3\text{O}_4$  (I),  $\text{Fe}_3\text{O}_4@\text{CQD}$  (II),  $\text{Fe}_3\text{O}_4@\text{CQD}@\text{Si}$  (III),  $\text{Fe}_3\text{O}_4@\text{CQD}@\text{Si}@\text{PNIPAM}$  (IV), and  $\text{Fe}_3\text{O}_4@\text{CQD}@\text{Si}@\text{PNIPAM}-\text{NH}_2/\text{Pd}$  (VI) obtained by DLS method according to size distribution data analysis. The  $\text{Fe}_3\text{O}_4$  nanoparticles had an average size of 134 nm and relatively low size dispersion (Figure 6a). The average size of  $\text{Fe}_3\text{O}_4@\text{CQD}$  is 178 nm (Figure 6b),  $\text{Fe}_3\text{O}_4@\text{CQD}@\text{Si}$  is 674 nm (Figure 6c),  $\text{Fe}_3\text{O}_4@\text{CQD}@\text{Si}@\text{PNIPAM}$  is 1160 nm (Figure 6d), and  $\text{Fe}_3\text{O}_4@\text{CQD}@\text{Si}@\text{PNIPAM}-\text{NH}_2/\text{Pd}$  is 1304 nm (Figure 6e). This indicates that the binding of PNIPAM chains onto  $\text{Fe}_3\text{O}_4$  nanoparticles and bonding of palladium to polymer chains increase their size.

Dispersion of the nanoparticles and their respective colloidal stability is associated with the surface electric charge of the NPs. Zeta potential measurements revealed value of -33.2 mV for  $\text{Fe}_3\text{O}_4$  (I), -39.8 mV for  $\text{Fe}_3\text{O}_4@\text{CQD}$  (II), -49.7 mV for  $\text{Fe}_3\text{O}_4@\text{CQD}@\text{Si}$  (III), -54.1 mV for  $\text{Fe}_3\text{O}_4@\text{CQD}@\text{Si}@\text{PNIPAM}$  (IV) and, -57.4 mV for  $\text{Fe}_3\text{O}_4@\text{CQD}@\text{Si}@\text{PNIPAM}-\text{NH}_2/\text{Pd}$  (VI) in water dispersion (see supporting information).  $\text{Fe}_3\text{O}_4$  NPs have smaller negative charge on the surface compare to coated  $\text{Fe}_3\text{O}_4$  which demonstrate fewer stability and higher tendency to agglomerate over time and form a core structure.

In contrast, the  $\text{Fe}_3\text{O}_4@\text{CQD}@\text{Si}@\text{PNIPAM}$  nanoparticles have more stability and fewer tendency for agglomeration because of the repulsive force between the particles, which is expressed by a more negative surface charge of the particles. Therefore, it is believed that larger negative surface charge has enhanced the colloidal stability of nanoparticles. The XRD patterns of the prepared  $\text{Fe}_3\text{O}_4$  MNPs (I),  $\text{Fe}_3\text{O}_4@\text{CQD}$  (II),  $\text{Fe}_3\text{O}_4@\text{CQD}@\text{Si}$  (III), and  $\text{Fe}_3\text{O}_4@\text{CQD}@\text{Si}@\text{PNIPAM}$  (IV) confirm the formation of inverse spinel crystal structure of magnetite  $\text{Fe}_3\text{O}_4$ . The position and also respective intensity of all detected diffraction peaks are the same as with JCPDS Card No. 75-0033 properly (Figure 7).

The diffraction peaks corresponding to  $2\theta=30.3^\circ$ ,  $35.65^\circ$ ,  $43.35^\circ$ ,  $53.4^\circ$ ,  $57.5^\circ$  and  $62.95^\circ$  manifested by their indices (210), (311), (400), (422), (511), and (440), respectively, are characteristic peaks of the  $\text{Fe}_3\text{O}_4$  nanoparticles. The quite identical diffraction peaks of compounds (II, III, and IV) with  $\text{Fe}_3\text{O}_4$  (I) suggest that the modification procedure had not affected the positions of the peaks and also particles crystal structure. Using the Scherrer equation, the crystallite size of  $\text{Fe}_3\text{O}_4$  nanoparticles (I) (Figure 7a),  $\text{Fe}_3\text{O}_4@\text{CQD}$  (II) (Figure 7b),  $\text{Fe}_3\text{O}_4@\text{CQD}@\text{Si}$  (III) (Figure 7c) and,  $\text{Fe}_3\text{O}_4@\text{CQD}@\text{Si}@\text{PNIPAM}$  (IV) (Figure 7d) were found to be about 138, 193, 308 and, 430 nm, respectively.



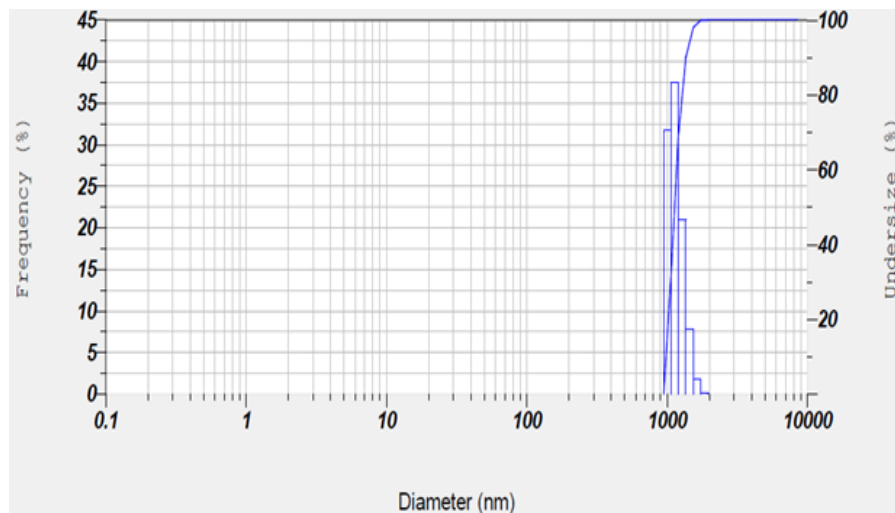


**Figure 6.** DLS of (a)  $\text{Fe}_3\text{O}_4$  MNPs (I), (b)  $\text{Fe}_3\text{O}_4@\text{CQD}$  (II), (c)  $\text{Fe}_3\text{O}_4@\text{CQD}@\text{Si}$  (III), (d)  $\text{Fe}_3\text{O}_4@\text{CQD}@\text{Si}@\text{PNIPAM}$  (IV), and (e)  $\text{Fe}_3\text{O}_4@\text{CQD}@\text{Si}@\text{PNIPAM}@\text{hydrazine}/\text{Pd}$  (VI)

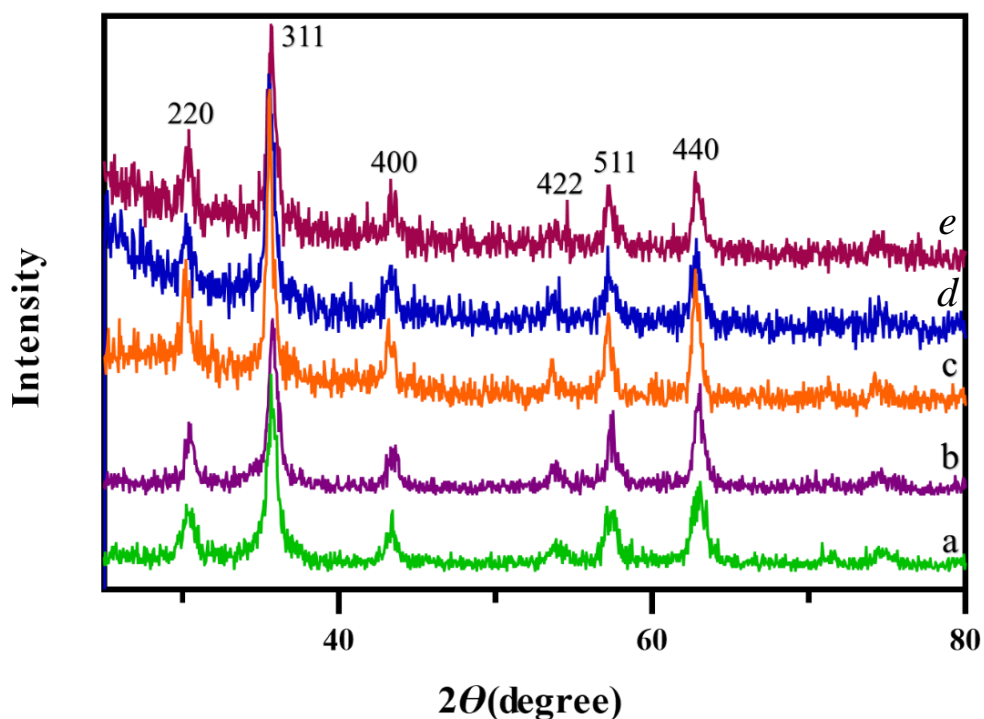


**Figure 7.** XRD patterns of (a)  $\text{Fe}_3\text{O}_4$  (I), (b)  $\text{Fe}_3\text{O}_4@\text{CQD}$  (II), (c)  $\text{Fe}_3\text{O}_4@\text{CQD}@\text{Si}$  (III), (d)  $\text{Fe}_3\text{O}_4@\text{CQD}@\text{Si}@\text{PNIPAM}$  (IV), and (e)  $\text{Fe}_3\text{O}_4@\text{CQD}@\text{Si}@\text{PNIPAM}-\text{NH}_2/\text{Pd}$  (VI)

#### *Application of $\text{Fe}_3\text{O}_4@\text{CQD}@\text{Si}@\text{PNIPAMNH}_2/\text{Pd}$ catalyst in Heck coupling reaction*

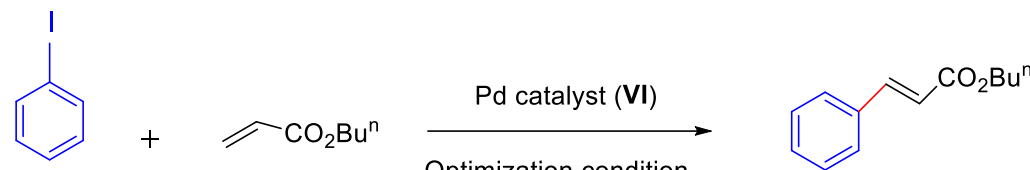
To check the potency of the designed Pd catalyst (VI), it was explored in the Heck cross-

coupling reaction of various haloarenes with *n*-butyl acrylate or styrene. To optimize the reaction conditions, the reaction between iodobenzene with *n*-butyl acrylate was firstly investigated as a model reaction for catalyst (VI).

The results are presented in Table 1. Initially, we investigate the impact of various bases ( $K_2CO_3$ ,  $NEt_3$ ,  $Na_2CO_3$ ,  $KOH$ , and  $NaOH$ ) and solvents (DMF,  $H_2O$ ,  $EtOH$ , toluene,  $DMF/H_2O$ , and  $EtOH/H_2O$ ), various temperature from 55 to 120 °C and varying amount of Pd catalyst (2-20 mg) to determine how the divers condition affected the outcomes. Rising the temperature from 55 °C to 95 °C improved the yield of the product, but there was not any significant improvement by changing the temperature from 95 °C to 120 °C (Table 1, entry 1-3). Among the solvents including  $EtOH$ ,  $EtOH/H_2O$  (1:1), toluene, DMF,  $DMF/H_2O$  (1:1), and  $H_2O$ , DMF yield the most percent of the product in 1 hour (entry 5 and entries 7-11). Base free condition (entry 16)

indicates that Heck reaction needs a base for reaction progress. Among various bases tested,  $K_2CO_3$  provided a higher yield (entry 5). Other bases like  $Na_2CO_3$ ,  $KOH$ ,  $NaOH$ , and  $NEt_3$  were explored and proved lower efficiency (entries 12-15). In addition, we investigated the influence of Pd catalyst amount on the coupling reaction between phenyl iodide and *n*-butyl acrylate (entries 2 and 4-6). The catalyst loading can be decreased to 2 mg Pd by extending the time of the reaction to 120 min and 80% conversion of iodobenzene was obtained. Eventually, the optimal conditions for this Pd catalyst were determined to be 5 mg of catalyst in DMF and  $K_2CO_3$  as a base at 95 °C.

**Table 1.** Optimization of base, solvent, and amount of catalyst for the reaction of iodobenzene with *n*-butyl acrylate in the presence of Pd catalyst (VI)<sup>a</sup>



Pd catalyst (VI)  
Optimization condition

Entry	Solvent	Base	Temperature (°C)	Amount of catalyst (mg)	Time (min)	Conversion (%) <sup>b</sup>
1	DMF	$K_2CO_3$	55	20	120	25
2	DMF	$K_2CO_3$	95	20	30	95
3	DMF	$K_2CO_3$	120	20	30	93
4	DMF	$K_2CO_3$	95	10	60	80
5	DMF	$K_2CO_3$	95	5	60	95
6	DMF	$K_2CO_3$	95	2	120	80
7	$H_2O$	$K_2CO_3$	95	5	60	0
8	$DMF/H_2O$ (1:1)	$K_2CO_3$	95	5	60	45
9	$EtOH$	$K_2CO_3$	95	5	60	20
10	$EtOH/H_2O$ (1:1)	$K_2CO_3$	95	5	60	0
11	Toluene	$K_2CO_3$	95	5	60	30
12	DMF	$NEt_3$	95	5	120	60
13	DMF	$Na_2CO_3$	95	5	120	30
14	DMF	$KOH$	95	5	120	25
15	DMF	$NaOH$	95	5	120	40
16	DMF	-	95	5	120	0

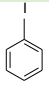
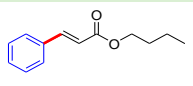
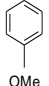
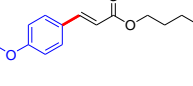
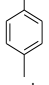
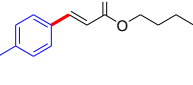
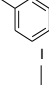
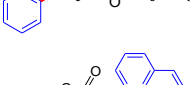
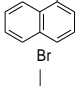
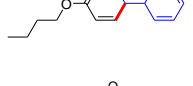
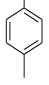
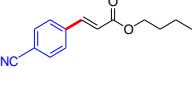
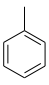
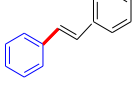
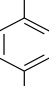
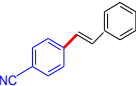
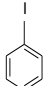
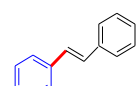
<sup>a</sup>Reaction conditions: iodobenzene (1 mmol), *n*-butyl acrylate (1.2 mmol), base (2 mmol), and 2 mL of solvent at 55-120 °C

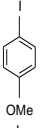
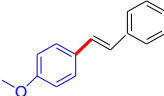
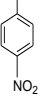
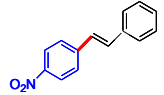
<sup>b</sup>Conversions based on iodobenzene

To probe the efficiency of the developed Pd catalyst, the Mizoroki-Heck cross-coupling reaction of several haloarenes with *n*-butyl acrylate (*n*-Bu acrylate) or styrene (St) was conducted and a range of substituted alkenes yielded. The reaction was carried out in DMF in the presence of  $K_2CO_3$  and Pd catalyst at 95 °C. Applying Pd catalyst, coupling reactions between various aryl halides and *n*-Bu acrylate or St demonstrated the universality of this

reaction system (Table 2). Aryl iodides with electron-deficient and electron-rich substitutes react well with *n*-butyl acrylate and styrene to create products with high-quality outcomes. Electron-withdrawing groups shorten the time of the reaction, whereas electron-donating groups lengthen it. Thus, for example, 1-iodo-4-nitrobenzene react more quickly than 4-iodotoluene in the reaction with styrene (Table 2, entries 9 and 11).

**Table 2.** Heck reaction of *n*-butyl acrylate or styrene with different aryl halides in the presence of Pd catalyst (VI)

Entry	Aryl halide	Alkene	Product	Time (min)	Isolated yield (%) <sup>b</sup>	TON <sup>c</sup>	TOF (min <sup>-1</sup> ) <sup>d</sup>
1		<i>n</i> -Bu acrylate		60	95	172	2.87
2		<i>n</i> -Bu acrylate		90	90	163	1.81
3		<i>n</i> -Bu acrylate		60	91	165	2.75
4		<i>n</i> -Bu acrylate		60	92	167	2.78
5		<i>n</i> -Bu acrylate		150	85	154	1.02
6		<i>n</i> -Bu acrylate		30	95	172	5.7
7		St		40	94	170	4.25
8		St		30	90	163	5.43
9		St		45	88	160	3.55

10		St		90	85	154	1.71
11		St		30	95	172	5.73

<sup>a</sup>Reaction conditions: Ar-x (1.0 mmol), olefin (1.2 mmol), K<sub>2</sub>CO<sub>3</sub> (2.0 mmol), and 2 mL of DMF at 95 °C, and 5 mg catalyst

<sup>b</sup>The characterization of products was performed by comparison of the <sup>1</sup>H-NMR of the products with authentic samples

<sup>c</sup>TON = mmol of product/mmol of Pd in the catalyst

<sup>d</sup>TOF = TON/time (min)

## Conclusion

The present study reported the synthesis and characterization of Pd catalyst based on the modified thermo-responsive PNIPAM grafted Fe<sub>3</sub>O<sub>4</sub>@CQD@Si *via* conventional free radical polymerization technique. Initially, Fe<sub>3</sub>O<sub>4</sub> NPs were created by the co-precipitation method, and then CQD, as green and sustainable support, was used to coat Fe<sub>3</sub>O<sub>4</sub> NPs instead of the conventional SiO<sub>2</sub>. Chemical modification of Fe<sub>3</sub>O<sub>4</sub>@CQD with polymerizable groups was performed through the reaction with VTES. Finally, PNIPAM was grafted to the modified Fe<sub>3</sub>O<sub>4</sub>, and then it was modified with hydrazine to convert it to an amino ligand. The amino support was subsequently coupled with Pd through reaction with Pd(OAc)<sub>2</sub>, and then adding NaBH<sub>4</sub> as a reducing agent to obtain the heterogeneous catalytic system. All materials are characterized through a wide range of methods, such as FT-IR, XRD, CHN, SEM, DLS, zeta potential, VSM, and TGA analysis techniques. This catalytic system was optimized for producing a variety of substituted alkenes in Mizoroki-Heck coupling reaction in good to outstanding yield. Easy purification of the substituted alkenes due to the convenient recyclability of the catalyst is the main characteristic of this process.

## Acknowledgements

The authors would greatly have appreciated the partial support of this study by Shiraz University Research Council.

## Disclosure Statement

No potential conflict of interest was reported by the authors.

## Funding

This research did not receive any specific grant from funding agencies in the public, commercial, or not-for-profit sectors.

## Authors' Contributions

All authors contributed to data analysis, drafting, and revising of the paper and agreed to be responsible for all the aspects of this work.

## Orcid

Soheila Ghasemi

<https://orcid.org/0000-0003-4469-0333>

## References

- [1]. Christoffel F., Ward T.R. *Catal. Lett.*, 2018, **148**:489 [Crossref], [Google Scholar], [Publisher]
- [2]. Aryanasab F., Shabanian M., Laoutid F., Vahabi H. *Appl. Organomet. Chem.*, 2021,



- 35:e6198 [[Crossref](#)], [[Google Scholar](#)], [[Publisher](#)]
- [3]. Das P., Linert W. *Coord. Chem. Rev.*, 2016, **311**:1 [[Crossref](#)], [[Google Scholar](#)], [[Publisher](#)]
- [4]. a) Ghasemi S., Karim S. *Mater. Chem. Phys.*, 2018, **205**:347 [[Crossref](#)], [[Google Scholar](#)], [[Publisher](#)]; b) Taghavi R., Rostamnia S. *Chemical Methodologies*, 2022, **6**:629 [[Crossref](#)], [[Publisher](#)]
- [5]. Rezayati S., Hajinasiri R., Erfani Z. *Res. Chem. Intermed.* 2016, **42**:2567 [[Crossref](#)], [[Google Scholar](#)], [[Publisher](#)]
- [6]. Ford M.F. *Catalysis of Organic Reactions, Boca Raton.*, 2001, 672 [[Crossref](#)], [[Publisher](#)]
- [7]. Hartley F.R. *Springer Dordrecht: Netherlands.*, 1985, **6**:340 [[Crossref](#)], [[Google Scholar](#)], [[Publisher](#)]
- [8]. Rezayati S., Salehi E., Hajinasiri R., Sharif Abad S.A.S. *C. R. Chim.*, 2017, **20**:554 [[Crossref](#)], [[Google Scholar](#)], [[Publisher](#)]
- [9]. Alonso D.A., Baeza A., Chinchilla R., Gómez C., Guillena G., Pastor I.M., Ramón D.J. *Catalysts*, 2018, **8**:202 [[Crossref](#)], [[Google Scholar](#)], [[Publisher](#)]
- [10]. Snoussi Y., Bastide S., Abderrabba M., Chehimi M. *Ultrason. Sonochem.*, 2018, **41**:551 [[Crossref](#)], [[Google Scholar](#)], [[Publisher](#)]
- [11]. Trisha D., Hiroshi U., Mahasweta N. *J. Solid State Chem.*, 2018, **260**:132 [[Crossref](#)], [[Google Scholar](#)], [[Publisher](#)]
- [12]. Nouri F., Rostamizadeh S., Azad M. *Inorg. Chim. Acta.*, 2018, **471**:664 [[Crossref](#)], [[Google Scholar](#)], [[Publisher](#)]
- [13]. Bahadori M., Tangestaninejad S., Moghadam M., Mirkhani V., Mechler A., Mohammadpoor-Baltork I., Zadehahmadi F. *Microporous Mesoporous Mater.*, 2017, **253**:102 [[Crossref](#)], [[Google Scholar](#)], [[Publisher](#)]
- [14]. L Wang L.L., Zhu L.P., Bing N.C., Wang L.J., *J. Phys. Chem. Solids*, 2017, **107**:125 [[Crossref](#)], [[Google Scholar](#)], [[Publisher](#)]
- [15]. Yum E.K., Hong E.K. *Tetrahedron.*, 2017, **73**:6581 [[Crossref](#)], [[Google Scholar](#)], [[Publisher](#)]
- [16]. Ulusal F., Darendeli B., Erünal E., Egitmen A., Guzel B. *J. Supercrit. Fluids*, 2017, **127**:111 [[Crossref](#)], [[Google Scholar](#)], [[Publisher](#)]
- [17]. Tran T.P.N., Thakur A., Trinh D.X., Dao A.T.N., Taniike T. *Appl. Catal., A* 2018, **549**:60 [[Crossref](#)], [[Google Scholar](#)], [[Publisher](#)]
- [18]. Balinge, K.R., Khiratkar, A.G., Bhagat, P.R. *J. Organomet. Chem.*, 2018, **854**:131 [[Crossref](#)], [[Google Scholar](#)], [[Publisher](#)]
- [19]. Liua B., Suna S., Gaoa Z., Zhanga D., Bianb G., Qi b Y., Yanga X., Li C. *Colloids Surf. A: Physicochem. Eng. Asp.*, 2014, **456**:195 [[Crossref](#)], [[Google Scholar](#)], [[Publisher](#)]
- [20]. a) Yadollahzadeh K. *Journal of Medicinal and Nanomaterials Chemistry*, 2022, **4**:144 [[Crossref](#)], [[Publisher](#)]; b) Yadollahzadeh, K. *Journal of Medicinal and Nanomaterials Chemistry*, 2021, **3**:81 [[Crossref](#)], [[Publisher](#)]; c) Khazaei R., Khazaei A., Nasrollahzadeh M. *Journal of Applied Organometallic Chemistry*, 2023, **3**:123 [[Crossref](#)], [[Publisher](#)]
- [21]. a) Esmaeilpoura M., Zahmatkesh S. *Inorg. Nano-Met. Chem.*, 2019, **49**:267 [[Crossref](#)], [[Google Scholar](#)], [[Publisher](#)]; b) Moghimi A., Abniki M. *Advanced Journal of Chemistry, Section A*, 2021 **4**:78 [[Crossref](#)], [[Publisher](#)]; c) Alinezhad H., Hajiabbas Tabar Amiri P., Mohseni Tavakkoli S., Muhiebes R., Fakri Mustafa Y. *Journal of Chemical Reviews*, 2022, **4**:288 [[Crossref](#)], [[Publisher](#)]
- [22]. Rezayati S., Kalantari F., Ramazani A. *RSC Adv.*, 2023, **13**:12869 [[Crossref](#)], [[Google Scholar](#)], [[Publisher](#)]
- [23]. Hadikhani S., Rekavandi M., Hosseinkhah S.M., Hajinasiri R., Rezayati S. *Iran J. Sci. Technol. Trans. Sci.*, 2018, **42**:1233 [[Crossref](#)], [[Google Scholar](#)], [[Publisher](#)]
- [24]. Ezzatzadeh E. *Journal of Medicinal and Nanomaterials Chemistry*, 2023, **4**:213 [[Crossref](#)], [[Publisher](#)]

- [25]. Zhou L., Gao C., Xu W. *Langmuir*, 2010, **26**:11217 [[Crossref](#)], [[Google Scholar](#)], [[Publisher](#)]
- [26]. Wang D., Liu W., Bian F., Yu W. *New J. Chem.*, 2015, **39**:2052 [[Crossref](#)], [[Google Scholar](#)], [[Publisher](#)]
- [27]. Aghahosseini H., Saadati M.R., Rezaei S.J.T., Ramazani A., Asadi N., Yahiro H., Mori M., Shajari N., RezaKazemizadeh A.R. *Sci. Rep.*, 2021, **11**:10239 [[Crossref](#)], [[Google Scholar](#)], [[Publisher](#)]
- [28]. Tamami B., Ghasemi S. *J. Mol. Catal. A: Chem.*, 2010, **322**:98 [[Crossref](#)], [[Google Scholar](#)], [[Publisher](#)]
- [29]. Tamami B., Farjadian F., Ghasemi S., Allahyari H., Mirzadeh M. *J. Braz. Chem. Soc.*, 2015, **26**:1591 [[Crossref](#)], [[Google Scholar](#)], [[Publisher](#)]
- [30]. Ghasemi S., Karim S. *Colloid Polym. Sci.*, 2018, **296**:1323 [[Crossref](#)], [[Google Scholar](#)], [[Publisher](#)]
- [31]. Tamami B., Farjadian F., Ghasemi S., Allahyari H. *New J. Chem.*, 2013, **37**:2011 [[Crossref](#)], [[Google Scholar](#)], [[Publisher](#)]
- [32]. Desmond L.J., Phan A.N., Gentile P. *Environmental Science. Nano*, 2021, **8**:848 [[Crossref](#)], [[Google Scholar](#)], [[Publisher](#)]

**How to cite this manuscript:** Soheila Ghasemi\*, Fatemeh Badri, Hadih Rahbar Kafshboran. Pd Catalyst Supported Thermo-Responsive Modified Poly(*N*-isopropylacrylamide) Grafted Fe<sub>3</sub>O<sub>4</sub>@CQD@Si in Heck Coupling Reaction. *Asian Journal of Green Chemistry*, 8(1) 2024, 39-56.  
DOI: 10.48309/ajgc.2024.408188.1401